NCAR
Research Aviation Facility

Bulletin No. 23

MEASUREMENT TECHNIQUES: AIR MOTION SENSING

rev. 11/89

D. H. Lenschow and P. Spyers-Duran

Note: At this time NCAR operates only one aircraft, a C-130Q Hercules (tail number N130AR). NCAR operated the three aircraft mentioned in this Bulletin when it was written in 1989. The basic equipment and instrumentation, equations and principles discusssed here are still pertinent and being used at our facility.

1. INTRODUCTION

NCAR presently operates three aircraft equipped with inertial navigation systems (INS) and a gust probe or a radome with pressure ports for air motion measurements. These aircraft (King Air, Sabreliner, and Electra) can be instrumented to measure both mean horizontal wind and turbulent fluctuations of the three air velocity components. The components are obtained by subtracting the velocity of the airplane, measured by the INS, from the velocity of the air, measured by the radome or gust probe. Since the flow measurements are in the aircraft frame of reference, these measurements are first converted to the earth's frame of reference by using the three airplane attitude angles measured by the INS, and are then subtracted from the airplane velocity components, which are obtained from integrated accelerometer outputs (corrected for Coriolis accelerations) in an earth-based frame of reference. Most applications of air-motion sensing systems involve either

(1) measurement of the mean horizontal wind, which is useful mainly for synoptic or mesoscale meteorological experiments, or
(2) measurement of high-frequency fluctuations of all three velocity components, which are used mainly to calculate turbulence statistics such as variances, and turbulence fluxes of heat, moisture, momentum, and turbulence energy.

2. AIR VELOCITY EQUATIONS

In this section we derive the equations for calculating the air velocity components from the INS and the flow-sensing probes. The derivation is similar to Axford's (1968). However, the terminology and coordinate systems are modified to conform to standard aeronautical engineering usage (Etkin, 1959) for the aircraft coordinate system and to standard inertial navigation (Kayton and Fried, 1969) and meteorological usage for the air velocity in the local earth coordinate system.

The velocity of the air with respect to the earth, $\boldsymbol{V = iu + jv + kw}$, is obtained by adding the velocity of the aircraft with respect to the earth, $\boldsymbol{v_p}$, and the velocity of the air with respect to the aircraft, $\boldsymbol{v_a}$. If all the measurements are made at the same point, we have

$$\vec{v} = \vec{v}_p + \vec{v}_a \qquad (2.1)$$

The components of $\boldsymbol{v_a}$ are measured with sensors mounted on the aircraft, either on a boom forward of the aircraft to reduce the effects of the distortion of the airflow by the aircraft or alternatively, from pressure ports on a radome to take advantage of the pressure differences produced by asymmetric flow about the aircraft's nose. On the NCAR aircraft the components of $\boldsymbol{v_p}$ are obtained from the integrated outputs of accelerometers mounted on the stabilized platform of an INS. Alternatively, $\boldsymbol{v_p}$ could be obtained from radiation transmitting and receiving devices, such as Doppler radars or radar altimeters, or from radio or radar navigation techniques.

If the aircraft velocity is obtained from integrated accelerometer outputs, the velocity is measured in an inertial frame of reference. In an earth-based coordinate system, we have

$$\frac{d\vec{v}_p}{dt} = \vec{a} - (\vec{\omega}_p + \vec{\omega}_e) \times \vec{v}_p + \vec{g} \qquad (2.2)$$

where

$\vec{a}$ is the measured acceleration
$\vec{\omega}_e$ and $\vec{\omega}_p$ are the angular velocities of the earth and platform, respectively; and
$\vec{g}$ is the gravitational acceleration (which includes the centripetal acceleration).

Since the accelerometers may not be collocated with the air velocity sensors, it may be necessary to add the term $\vec{\Omega}_p \times \vec{R}$ to (2.2), where $\vec{\Omega}_p$ is the angular acceleration of the aircraft and $\boldsymbol{R = iX + jY + kZ}$ is the distance from the accelerometers to the air velocity sensors. Thus, (2.1) can be combined with the integral of (2.2) and rewritten as

$$\vec{v} = \vec{v}_a + \int \left[\vec{a} - (\vec{\omega}_p + \vec{\omega}_e) \times \vec{v}_p + \vec{g}\right] dt + \vec{\Omega}_p \times \vec{R} = \vec{v}_a + \vec{v}_p + \vec{\Omega}_p \times \vec{R} \qquad (2.3)$$

In the general case, the measured components of $\boldsymbol{v_a}$ and $\boldsymbol{v_p}$ may not be in the local earth coordinate system. The airflow sensors, for example, are usually rigidly connected to the aircraft fuselage. Therefore, it is necessary to know the angles between the coordinates of the airflow sensors and the local earth coordinates. The measured velocity components can then be rotated by means of the appropriate angular transformation to the local earth axes so that the rotation angles of the platform gimbals are equivalent to the aircraft attitude angles. From the inside platform gimbal outward, i.e., from the stabililzed accelerometer and gyro cluster outward to the aircraft frame, the order of the rotations is as follows: first, a rotation ψ, about the z-axis of the earth coordinate system; second, a rotation θ, about the y'-axis, which is the y-axis rotated in the horizontal plane by the angle ψ ; and third, a rotation ϕ, about the x'-axis, which is the x-axis in the aircraft coordinate system. The aircraft axes are shown in Fig. 2.1; a right-handed angular rotation is positive. The symbols and axes have been defined to correspond to standard aerodynamic conventions (Etkin, 1959).

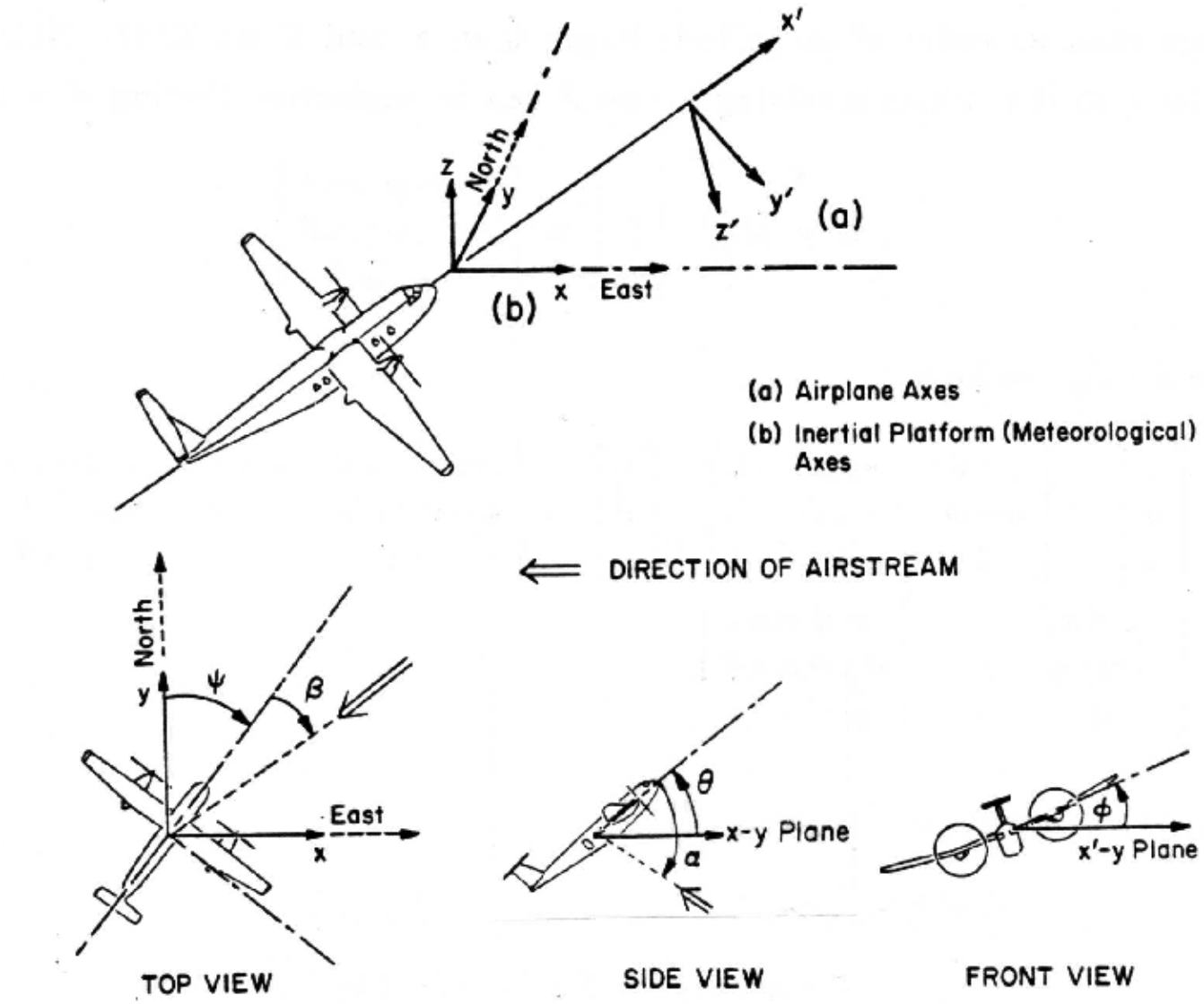

Fig. 2.1. Top: Coordinate systems used in deriving equations for calculating the air velocity components. Bottom: Airplane attitude angles and axes used in equations for calculating the air velocity components.

In matrix notation, the transformation of the air velocity from aircraft (x', y', z') to platform (x, y, z) coordinates {same as (b) coordinates in Fig. 2.1} is given by

$$[u_i] = [T_{ij}] \cdot [u'_j] \qquad (2.4)$$

where

$$[T_{ij}] = \begin{bmatrix} \cos\psi & -\sin\psi & 0 \\ \sin\psi & \cos\psi & 0 \\ 0 & 0 & 1 \end{bmatrix} \cdot \begin{bmatrix} \cos\theta & 0 & \sin\theta \\ 0 & 1 & 0 \\ -\sin\theta & 0 & \cos\theta \end{bmatrix} \cdot \begin{bmatrix} 1 & 0 & 0 \\ 0 & \cos\phi & -\sin\phi \\ 0 & \sin\phi & \cos\phi \end{bmatrix} \qquad (2.5)$$

$$= \begin{bmatrix} \cos\psi\cos\theta & -\sin\psi\cos\phi + \cos\psi\sin\theta\sin\phi & \sin\psi\sin\phi + \cos\psi\sin\theta\cos\phi \\ \sin\psi\cos\theta & \cos\psi\cos\phi + \sin\psi\sin\theta\sin\phi & \sin\psi\sin\theta\cos\phi - \cos\psi\sin\phi \\ -\sin\theta & \cos\theta\sin\phi & \cos\theta\cos\phi \end{bmatrix} \qquad (2.6)$$

The terms of $\vec{\Omega}_p \times \vec{R}$ must also be transformed to the local earth coordinate system. ***X*** is more than an order of magnitude larger than ***Y*** and ***Z*** on all the NCAR aircraft installations, so that terms involving ***Y*** and ***Z*** can be neglected. Setting ***X = L***, we have

$$[R_i] = [T_{ij}] \cdot \begin{bmatrix} L \\ 0 \\ 0 \end{bmatrix} = \begin{bmatrix} L\cos\psi\cos\theta \\ L\sin\psi\cos\theta \\ -L\sin\theta \end{bmatrix} \qquad (2.7)$$

Similarly for $\vec{\Omega}_p$ we have

$$[\Omega_{p_i}] = \begin{bmatrix} 0 \\ 0 \\ \dot{\psi} \end{bmatrix} + \begin{bmatrix} \cos\psi & -\sin\psi & 0 \\ \sin\psi & \cos\psi & 0 \\ 0 & 0 & 1 \end{bmatrix} \cdot \begin{bmatrix} 0 \\ \dot{\theta} \\ 0 \end{bmatrix} + \begin{bmatrix} \cos\psi\cos\theta & -\sin\psi & \cos\psi\sin\theta \\ \sin\psi\cos\theta & \cos\psi & \sin\psi\sin\theta \\ -\sin\theta & 0 & \cos\theta \end{bmatrix} \cdot \begin{bmatrix} \dot{\phi} \\ 0 \\ 0 \end{bmatrix}$$
$$= \begin{bmatrix} -\dot{\theta}\sin\psi & + & \dot{\phi}\cos\psi\cos\theta \\ \dot{\theta}\cos\psi & + & \dot{\phi}\sin\psi\cos\theta \\ \dot{\psi} & - & \dot{\phi}\sin\theta \end{bmatrix} \qquad (2.8)$$

Thus, in vector notation,

$$\vec{\Omega} \times \vec{R} = L\left[\vec{i}(\dot{\theta}\sin\theta\cos\psi - \dot{\psi}\sin\psi\cos\theta) + \vec{j}(\dot{\psi}\cos\psi\cos\theta - \dot{\theta}\sin\psi\sin\theta) - \vec{k}\dot{\theta}\cos\theta\right] \qquad (2.9)$$

The angle of attack, α, is the angle of the airstream with respect to the aircraft in the aircraft's vertical plane, with α positive in the downward direction; the angle of sideslip, β, is the angle of the airstream with respect to the aircraft in the aircraft's horizontal plane, with clockwise (looking from above) rotation positive, as shown in Fig. 2.1. The air velocity components with respect to the aircraft are calculated by first correcting the measured true airspeed for angle of attack and sideslip sensitivities (See Section 4.); the magnitude of the corrected true airspeed is defined as U_a. We then rotate the airflow vector to the airplane coordinate system. If we first rotate through the angle α to the horizontal plane, then rotate to the longitudinal aircraft axis, the components of air velocity in the aircraft frame of reference are $-U_a D^{-1}$ along the ***x***'-axis, $-U_a D^{-1} \tan\beta$, along the ***y***'-axis, and $-U_a D^{-1} \tan\alpha$ along the ***z***'-axis, where $D = (1 + \tan^2\alpha + \tan^2\beta)^{1/2}$

> [This differs from the expressions given by Lenschow (1972). For small flow angles, however, the magnitudes of the differences are negligible. We are grateful to A. Weinheimer and J. Leise, who each independently pointed out the error and corrected the previous derivation.]

So far, the equations have been derived using standard aeronautical engineering terminology. In converting to a meteorological and inertial navigation frame of reference, we make the following changes: first, the sign of vertical velocity is changed so that ***w*** is positive in an upward direction; second, ψ, which now corresponds to the true heading, is measured from the ***y***-axis, or from north, and the ***z***-axis now points east, as shown in Fig. 3. As a result, ψ**(new)** = ψ**(old) - 90°**, ***v*(new) = - *v*(old)**, and ***w*(new) = - *w*(old)**. The final equations used for calculating the air velocity with respect to the earth are:

$$
\begin{aligned}
u &= -U_a D^{-1}[\sin\psi\cos\theta + \tan\beta(\cos\psi\cos\phi + \sin\psi\sin\theta\sin\phi) \\
&\quad + \tan\alpha(\sin\psi\sin\theta\cos\phi - \cos\psi\sin\phi)] + u_p - L(\dot{\theta}\sin\theta\sin\psi - \dot{\psi}\cos\psi\cos\theta) \\
v &= -U_a D^{-1}[\cos\psi\cos\theta - \tan\beta(\sin\psi\cos\phi - \cos\psi\sin\theta\sin\phi) \\
&\quad + \tan\alpha(\cos\psi\sin\theta\cos\phi + \sin\psi\sin\phi)] + v_p - L(\dot{\psi}\sin\psi\cos\theta + \dot{\theta}\cos\psi\sin\theta) \\
w &= -U_a D^{-1}(\sin\theta - \tan\beta\cos\theta\sin\phi - \tan\alpha\cos\theta\cos\phi) + w_p + L\dot{\theta}\cos\theta
\end{aligned}
\qquad (2.10)
$$

These are the exact equations that are used in the standard NCAR data processing routines for calculating the air velocity. For purposes of illustration, however, it can be shown that for approximate straight and level flight (i.e., when the pilot or autopilot attempts to keep the aircraft level, but air velocity fluctuations still cause perturbations in the aircraft velocity and attitude angles) many of the terms in (2.4) are negligible.

First we assume that terms involving the separation distance, L, are small. This is generally true if the separation distance is less than about 10 m and the aircraft is not undergoing a pilot-induced pitching maneuver. Next we make the following small-angle approximations: for the horizontal components, u and v, we assume that the cosines of α, θ and ϕ are unity; that terms that involve the products of sines of two of the above angles are negligible; and that $\tan(\alpha, \beta) \simeq \sin(\alpha, \beta)$. For the vertical component w, we make the same assumptions for the angles β, θ and ϕ. Equations (2.10) then reduce to a form commonly used for approximate calculations of the three velocity components,

$$
\begin{aligned}
u &= -U_a \sin(\psi + \beta) + u_p \\
v &= -U_a \cos(\psi + \beta) + v_p \\
w &= -U_a \sin(\theta - \alpha) + w_p
\end{aligned}
\qquad (2.11)
$$

We can estimate the required accuracy of attitude and airstream incidence angle measurements from (2.11). In order to obtain the mean horizontal wind, the angle ($\psi + \beta$) must be measured accurately. For a mean wind accuracy of 0.5 m/s and an aircraft speed of 100 m/s, this angle must be measured with an absolute accuracy of 0.005 radians, or 0.06°. A heading angle of this accuracy is difficult to measure with a standard aircraft magnetic compass. An INS, however, can measure true heading to well within this accuracy.

A reasonable figure for short-term velocity accuracy necessary to estimate turbulence fluctuations is 0.1 m/s. At an airplane speed of 100 m/s, the required angular accuracy for the first terms on the right side of (2.11) is 0.001 radians, or 0.060°. This can be a difficult requirement to meet. Fortunately, an INS has even more stringent accuracy requirements than this for accurate navigation, so attitude angles of this short-term accuracy can be measured.

3. DESCRIPTION OF INSTRUMENTATION

- Gust Probe Sensors

  The three air velocity components with respect to the airplane are obtained from measurements of the two airflow angles and the true airspeed. Figures 3.1 and 3.2 show the two types of sensors that are used on NCAR aircraft to measure the airflow angles; the differential pressure probe and the instrumented radome sense the pressure difference across a symmetric set of ports at varying how angles. On the differential pressure probe, airspeed is obtained from a differential pressure measurement across the dynamic and static ports of the probe.

Fig. 3.1a. The NCAR Sabreliner aircraft equipped with both the differential pressure probe (at the end of the boom) and the radome with pressure ports. Both are used to obtain flow angles by pressure difference measurements.

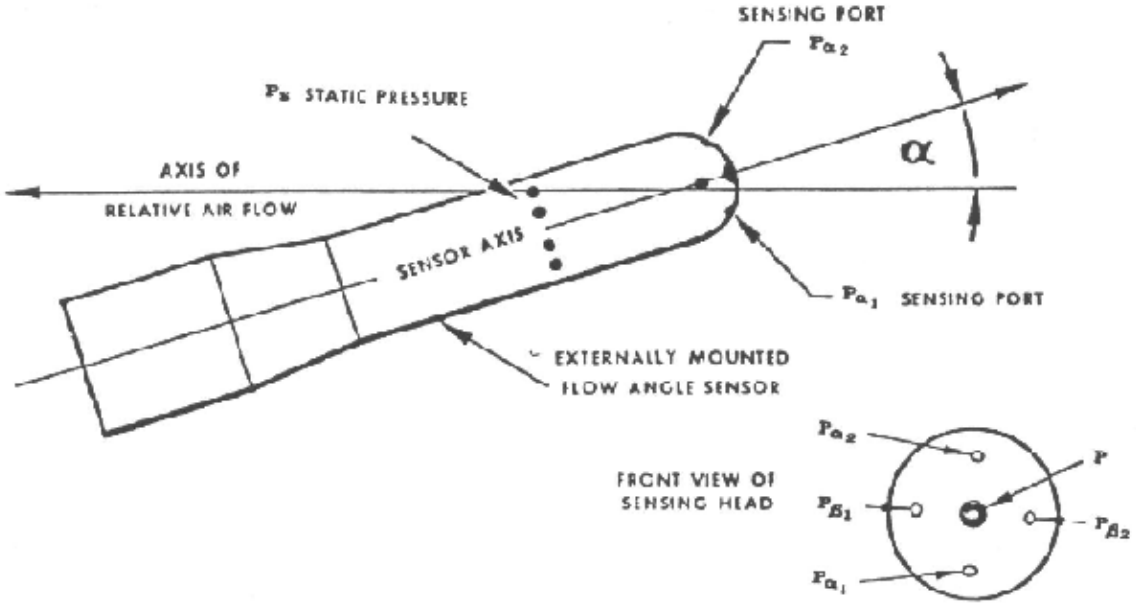

Fig. 3.1b. Schematic representation of the differential pressure probe manufactured by Rosemount Engineering, Inc., Model 858. Pressures at the ports are labeled on the figure.

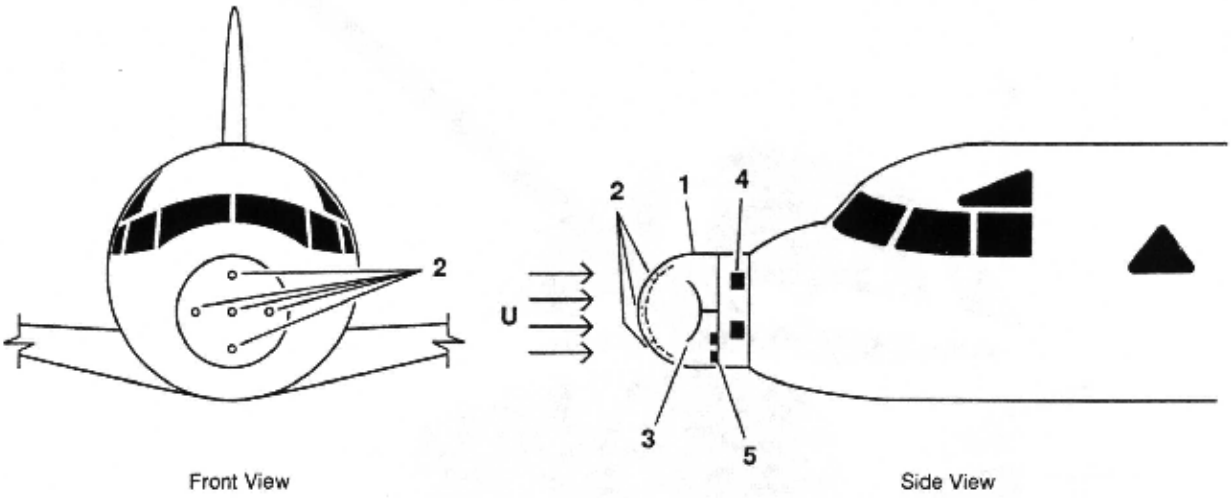

1. Radome with fluted deiced area
2. Differential pressure ports
3. Nose weather radar
4. Sensor mount pods
5. Pressure transducers

Fig. 3.2. Schematic views of radome differential pressure gust probe system.

- Differential Pressure Probe and Radome Technique

  An inevitable consequence of aircraft flight is distortion of the how in the vicinity of the aircraft. Therefore, any probe mounted on the aircraft is sensing in a perturbed flow field (Wyngaard et al., 1985). This means that for air velocity measurements using a boom-mounted gust probe, corrections must be made for the effects of this perturbation. These corrections are determined from the flight maneuvers discussed in Section 4. Alternatively, in the case of the radome technique, the pressure field resulting from the flow perturbations induced by the aircraft itself is used to obtain the flow angles. As discussed by Brown et al. (1983), for a hemispherically-shaped radome, this pressure difference is a nearly linear function of the flow angle.

The differential-pressure flow-angle sensor is constructed in the shape of a hemisphere capping a cylindrical tube (Fig. 3.1b). The flow around it leads to the pressure distribution shown in Fig. 3.3 when the tube axis is parallel to the flow. If the flow is at an angle with respect to the tube axis, the pressure distribution is no longer symmetric with respect to the tube axis. Thus, for a pair of ports symmetrically located above and below the tube axis, as in Fig. 3.3, an angular rotation causes an increased pressure in one port and a reduced pressure in the other. The net effect is a differential pressure between the top and bottom ports which is a function of flow angle and indicated airspeed. By placing a second pair of ports at right angles to the first, simultaneous measurements of both airflow angles with respect to local flow are obtained. Further details of the differential-pressure measuring technique are discussed by Brown et al. (1983).

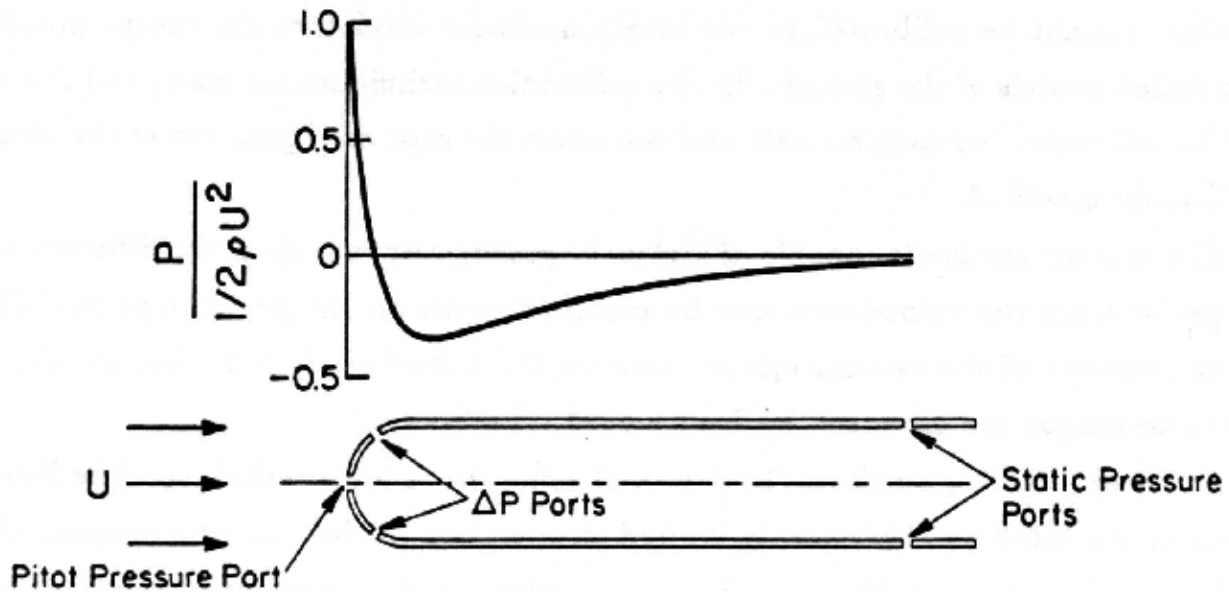

Fig. 3.3. Top: pressure distribution normalized by the dynamic pressure on the surface of a hemisphere-capped cylinder embedded in a uniform flow parallel to the axis of the cylinder. Bottom: A schematic cross-sectional view of the cylinder shows the arrangement of pressure sensing ports for sensing airflow angles, and Pitot and static pressures.

RAF currently has available an electrically-deiced differential-pressure probe (Rosemount Model No. 858AJ) for use on the Sabreliner aircraft. This probe can be used for limited measurements in clouds and in icing conditions. However, long flight legs in clouds or precipitation can lead to water accumulation in the pressure lines, which can cause errors in the pressure measurements. The probe has symmetric sets of holes drilled in the 2.8 cm-diameter hemisphere at an angle of 45° and a forward-looking port 0.14 cm in diameter. The probe also has a ring of static ports surrounding the cylindrical part of the probe 8.9 cm from the probe tip. Pressure differences are sensed by transducers mounted at the base of the nose boom connected to the ports by pressure lines. The inside diameter of the tubing inside the probe is 0.36 cm; the inside diameter of the lines connecting the probe tubing to the pressure transducer is 0.43 cm. The length of these pressure lines limits the instrument's frequency response. In the Sabreliner, for example, the tubing length is about 5 m. The time responses of both the dynamic pressure and the flow angle measurements on the Sabreliner with the differential pressure probe are discussed in Appendix A

The radome technique is similar, in principle, to the differential-pressure technique. The major difference is that the nose of the airplane itself is used as a probe instead of a separate flow angle sensor. Therefore, a nose boom is not needed for this technique. The technique cannot be calibrated in commonly-available wind tunnels, except possibly by using scaled models of the aircraft. In situ calibration techniques are used, and the system must be calibrated for each aircraft and whenever the nose configuration of the aircraft is significantly modified.

The radome system is capable of higher-frequency response than the differential pressure probe, since the transducers can be mounted closer to the pressure ports. The frequency response of the

radome system used on the Sabreliner is > 10 Hz. Details of the radome technique are discussed by Brown, et al. (1983). All three NCAR aircraft can be deployed using the radome technique. The Sabreliner radome is unheated and therefore is limited to operation in clear air and non-precipitating cloud. The King Air and Electra radomes are deiced and contain provisions for trapping ingested water; therefore, they can be used in all weather. Wind tunnel, flight test and theoretical analyses indicate that, for both the radome and the differential pressure probe technique, the flow angles are related to the pressure difference ΔP across the respective angle-sensing pressure ports. For the attack angle, α, this relation is

$$\alpha = \alpha_o + C_\alpha^{-1}\frac{(\Delta P)}{q} \qquad (3.1)$$

where q is the Pitot-static pressure difference, and α_o is a bias in the measured flow angle. The sensitivity coefficients $C_{\alpha,\beta}$ can be estimated from measurements of $(\Delta P)_{\alpha,\beta}$ at known values of q, as well as α or β. For the Rosemount 858AJ, $C_{\alpha,\beta} = C \simeq 0.079/°$ for Mach number, $M < 0.52$. This coefficient has been determined theoretically, as well as from wind tunnel calibrations conducted in the Cornell Aeronautical Laboratory (Andersen, 1955), and by the RAF in the U.S. Air Force Academy Subsonic Wind Tunnel. For $M > 0.52$, data obtained from the manufacturer indicate that C monotonically decreases to 0.056/° at $M = 0.9$. A fourth-order polynomial is used to approximate C for $0.52 <= M <= 0.90$.

The sensitivity coefficients for the radome differential pressure system have been determined from theoretical studies, flow model calculations (for the Electra), wind tunnel scale model studies (for the KingAir) and from the flight maneuvers discussed in Section 4, and are generally in close agreement; however, the flight-derived coeflicients are used in practice for calculating the three air velocity components. These values are listed in Table 1, along with the tube lengths between the pressure ports and the transducers, and the angles ϑ and φ , which are the angles between the ports and the longitudinal airplane axis in the vertical and horizontal planes, respectively.

Table 1
Sensitivity coefficients, pressure port attitude angles (ϑ for the attack angle and φ for the sideslip angle) and tube lengths for the radome differential pressure systems on all three NCAR aircraft. In all cases the tube diameter is 4.3 mm.

Aircraft	C_α/°	ϑ	C_β/°	φ	Tube length (m)
King Air (N312D)	0.08207	33°	0.07448	33°	0.7
Sabreliner (N307D)	0.0570	33°	0.0410	33°	1.8
Electra (N308D)	0.07155 $\alpha_o = 0.4095$	33°	0.06577 $\beta_o = 0.0375$	29°	3.5

The differential pressure transducers are calibrated on the airplane by applying known values of pressure difference across the pairs of probe ports.

- Pitot and Static Pressure Probes

All NCAR airplanes have dynamic or ram and static pressure ports for measuring dynamic (total - static) pressure q which is used to calculate airspeed. Rosemount Models 850L-2 and 852J Pitot-static tubes are mounted on the King Air and Electra wingtips; furthermore, the Rosemount Model 858AJ differential pressure probe (Fig. 3.1) already contains the necessary static and dynamic pressure ports. Dynamic pressure can also be measured at the front of the radomes,

although they are more sensitive to airflow angles than the Pitot-static tubes. These pressure ports are connected to pressure transducers, which are used to measure both the static pressure P_s, as well as q. As discussed in Appendix A, the 858AJ probe has longer pressure lines which limit its frequency response for pressure fluctuations to < 1 Hz on the Sabreliner.

The true airspeed is calculated from q, P_s and the measured temperature, T_r, by application of Bernoulli's equation for the conservation of energy in a compressible fluid. (See Appendix B for details.) The Mach number, M (which is the ratio of the true airspeed to the speed of sound), is calculated from the relation

$$M^2 = \frac{2}{\gamma - 1}\left[\left(\frac{q + P_s}{P_s}\right)^{\frac{\gamma-1}{\gamma}} - 1\right] \qquad (3.2)$$

where $\gamma = C_p/C_v$ is the ratio of the specific heat of air at constant pressure to the specific heat at constant volume. Then the true airspeed is obtained from the relation

$$U_a = \left[\frac{R\gamma T_r M^2}{1 + 0.5(\gamma - 1)r M^2}\right]^{1/2} \qquad (3.3)$$

where $r \equiv (T\text{r} - T\text{s})/(T_t - T_s)$ is the recovery factor of the thermometer, R is the gas constant (= 287.04 J/kg/K for dry air), T_s is the ambient air temperature, and T_t is the total air temperature which is the temperature attained by an adiabatic reduction of the air velocity to zero (with respect to the airplane).

- INS Measurements

The inertial navigation system (INS) consists of an orthogonal triad of accelerometers mounted on a gyrostabilized gimbaled platform which is kept level by continuous computation and application of the required torquing rates. These rates are determined by integrating the horizontal accelerometer outputs and applying corrections based on the earth's rate of rotation and the geographic coordinates of the platform. The geographic coordinates are obtained by a second integration of the accelerometer outputs, again with appropriate corrections. The two corrected horizontal velocity components are available from the INS computer. The vertical velocity is obtained from a counter that accumulates pulses from the vertical accelerometer. Thus the INS can provide measurements of the three airplane velocity components and, by recording the output of angular resolvers mounted on the platform gimbals, the three attitude angles of the airplane with respect to the earth.

The INS platform used by NCAR (Litton Systems, Inc. LTN-51) is not torqued about its vertical axis while operating in the navigation mode, and therefore the heading or azimuth of the platform remains constant in inertial space. In this mechanization, which is called a free-azimuth, or azimuth-wander system, platform heading in the earth-based coordinate system changes with time and with east-west displacement of the aircraft. Its initial heading is determined by the orientation of the INS during alignment; early in the alignment sequence the platform is caged so that the platform axes are aligned to the INS case. True heading, therefore, is a calculated variable, obtained initially by a computer gyrocompassing of the system. Thereafter, during navigation the INS calculates and continuously updates the true heading. In the LTN-51, the angle between true north and the x-component of the platform (along which u_e is measured) is called the azimuth-wander angle, ε, as shown in Fig. 3.4. The airplane velocity components in an earth-based (geographic) coordinate system are then calculated from the rotation

$$\begin{aligned} u_p &= -v_e \cos\varepsilon + u_e \sin\varepsilon \\ v_p &= v_e \sin\varepsilon + u_e \cos\varepsilon \end{aligned} \qquad (3.4)$$

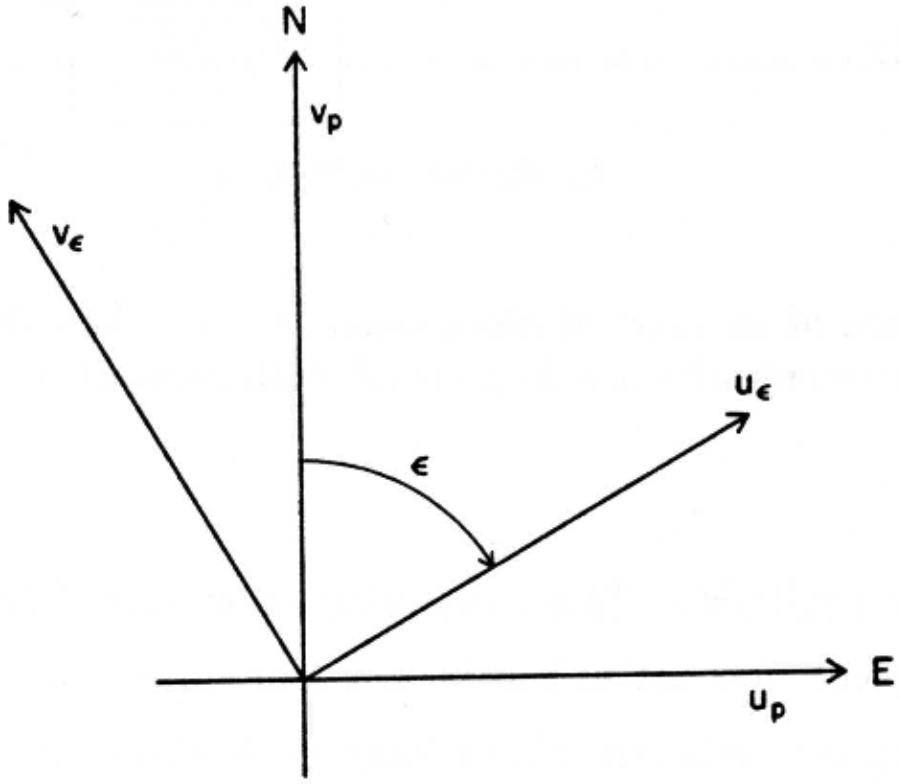

Fig. 3.4. Angular orientation of an azimuth-wander INS platform with respect to geographic coordinates.

The INS computer solves and integrates (2.2) in the horizontal plane of the local earth coordinate system; thus the instantaneous velocity and position are computed and can be displayed, along with related quantities, such as ground speed and drift angle, and range and bearing to selected targets or destinations. A block diagram of an inertial navigation system is shown in Fig. 3.5.

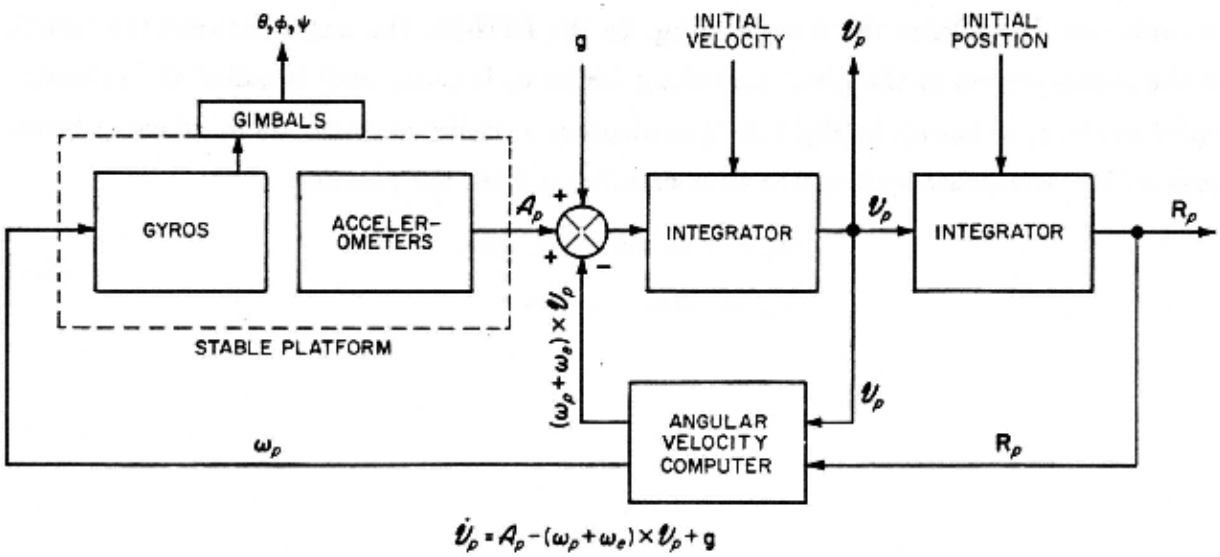

Figure 3.5. Block diagram of an inertial navigation system. The dashed rectangle represents the gimbaled stable element which is kept level with respect to local earth, and R_p is the position vector.

The inertial system's computer also calculates the angular velocity required to keep the platform level. Torque is then applied (by electromagnetic coupling) to the appropriate gyro axes perpendicular to the spin axes of the gyro. The angular velocity of the gyro rotor along an axis mutually perpendicular to both

the gyro spin axis and torque input axis is directly proportional to the applied torque. The axes of the stable platform are slaved to the gyro output axes by rotating the appropriate gimbals so that the angular deviation between the two sets of axes is negligible. Thus, the rotation angles of the gimbals are identical to the attitude angles of the aircraft in the local earth coordinate system. These angles are measured with dual-speed resolvers which have both single and eight-pole outputs. The outputs of each of the resolvers are thus approximately proportional to the sine and cosine of the attitude angle (for the single-pole output) and eight times the attitude angle (for the eight-pole output). Using the pitch angle θ as an example, $\theta/n = \tan^{-1}(E_1/E_2)$, where n is the number of poles and E_1 and E_2 are the sine and cosine outputs, respectively. In practice, the single-pole output is used to determine the octant of the eight-pole output, and the eight-pole output is used for the attitude angle measurement.

A complete error analysis of an inertial navigation system is complicated. However, several salient features can be easily demonstrated by considering a simplified two-dimensional case. As an example, we investigate the error propagation of an accelerometer bias error or an angular misalignment of the platform and an accelerometer or gyro drift error, assuming that the Coriolis terms of (2.2) can be neglected. The accelerometers along the horizontal axes sense an acceleration approximately equal to the angular deviation from the local geopotential surface δ, times g_0, which is the gravitational acceleration at some reference level, R_0, from the center of the earth. The inertial system's computer integrates this acceleration twice, changes its computed position a distance, ξ; and rotates the platform through an angle ξ/R_0. Thus, the acceleration sensed by the inertial system is

$$\ddot{\xi} = g_o(\delta - \xi/R_o) = -(g_o/R_o)\xi + \epsilon_x \qquad (3.5)$$

where ϵ_x is the acceleration error.

Along the vertical axis, the gravitational acceleration as a function of the vertical displacement, ζ, away from some reference level and the latitude can be obtained from the equation

$$\begin{aligned} g(\zeta) &= g(1 + \zeta/R_o)^{-2}(1 + 0.00529\sin^2\lambda) \\ &\simeq g_o(1 - 2\zeta/R_o)(1 + 0.00529\sin^2\lambda)\text{cm s}^{-2} \end{aligned} \qquad (3.6)$$

According to Kayton and Fried (1969), this equation is accurate to within 0.02 cm/s^2 at sea level. The resulting equations for horizontal and vertical position errors (neglecting the latitudinal variation of g) are

$$\begin{aligned} \ddot{\xi} + \omega_s^2\xi &= \epsilon_x \\ \ddot{\zeta} - 2\omega_s^2\zeta &= \epsilon_z \end{aligned} \qquad (3.7)$$

where $\omega_s = \sqrt{g_o/R_o} = 1.24 \times 10^{-3}$ rad/s (equivalent to a period of 84.4 min, known as the Schuler period). The major effect of the neglected Coriolis terms involving u_p and v_p, which are typically about 10% of ω_s, is to divide the horizontal error into two sinusoidal components with angular velocities of approximately $\omega_s \pm (1/2)(\omega_z + \Omega \sin\lambda)$.

Thus, the two sinusoidal components added together result in a modulated error with a carrier frequency of ω_s and a modulation frequency of $(1/2)(\omega_z + \Omega \sin\lambda)$.

As an example, we assume

$$\epsilon_x = \epsilon_z = \begin{cases} 0, & t<0 \\ a_o + a_1 t & t\geq 0 \end{cases}$$

$$\xi(0) = \zeta(0) = \dot{\xi}(0) = \dot{\zeta}(0) = 0 \qquad (3.8)$$

The solutions of (3.8) for the velocity error are

$$\dot{\xi} = \frac{a_o \sin \omega_s t}{\omega_s} + \frac{a_1}{\omega_s^2}(1 - \cos \omega_s t)$$
$$\dot{\zeta} = \frac{a_o \sinh \sqrt{2\omega_s t}}{2\omega_s} - \frac{a_1}{2\omega_s^2}(1 - \cosh \sqrt{2\omega_s t}) \qquad (3.9)$$

As can be seen, the vertical velocity error diverges rapidly. To compare the two errors, we assume $a_0 = 2 \times 10^{-2}$ cm/s^2 and $a_1 = 2 \times 10^{-5}$ cm/s^3. Substituting these values into (3.9), we obtain

$$\dot{\xi} = 16 \sin \omega_s t + 13(1 - \cos \omega_s t) \text{ cm s}^{-1}$$
$$\dot{\zeta} = 8 \sinh \sqrt{2\omega t_s} - 6(1 - \cosh \sqrt{2\omega_s t}) \text{ cm s}^{-1} \qquad (3.10)$$

These variables are plotted in Fig. 3.6.

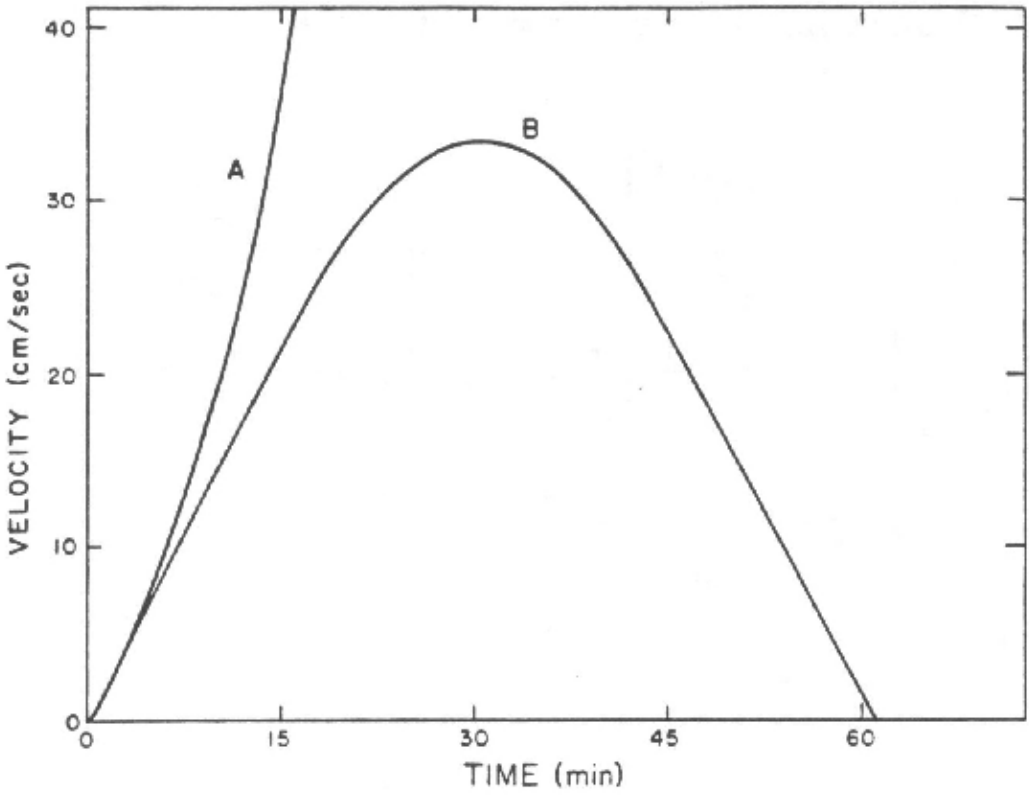

Fig. 3.6. Velocity errors in an inertial navigation system. (The error-generating function is described in text.) Curve A-vertical velocity, curve B-horizontal velocity.

The position errors, i.e., the integrals of (3.10) are

$$\xi = 130\left[1 - 1.3 \sin(\omega_s t + 51°) + 10^{-3} t\right] m$$
$$\zeta = 46(\cosh \sqrt{2}\omega_s t - 1) + 37 \sinh \sqrt{2}\omega_s t - 0.06tm \qquad (3.11)$$

These variables are plotted in Fig. 3.7.

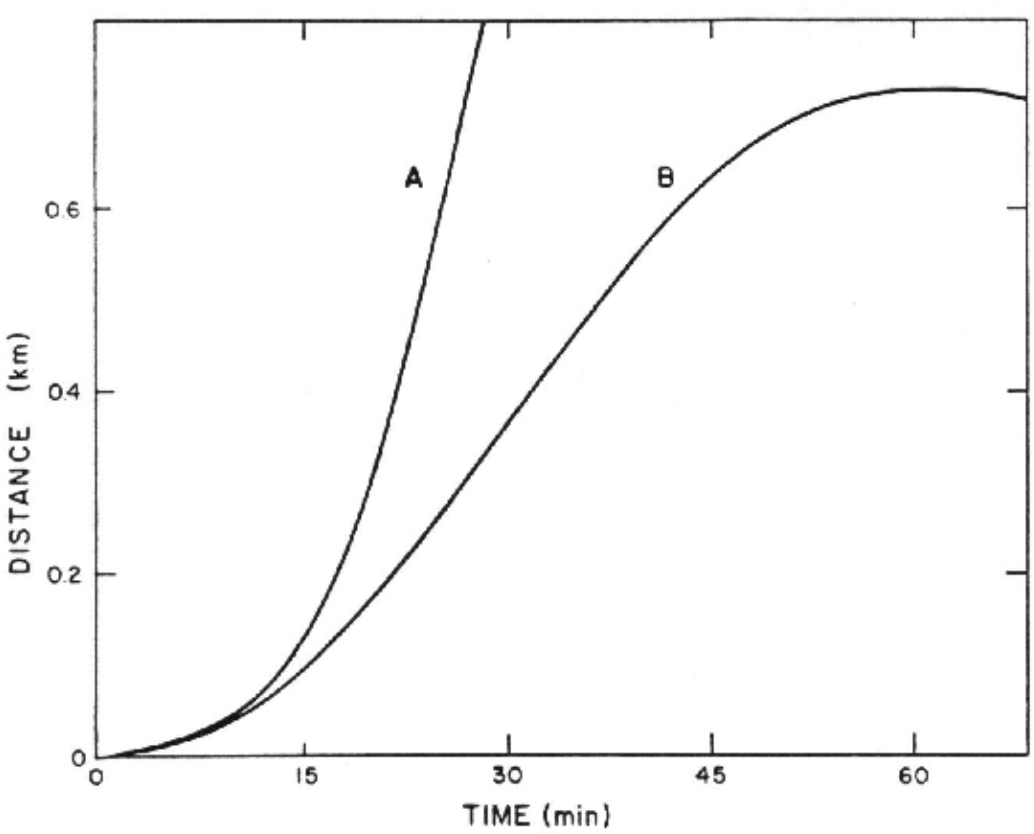

Fig. 3.7. Position errors in an inertial navigation system. (The error-generating function is described in text.) Curve A-inertial altitude, curve B-horizontal position.

Other errors in position and velocity exist as well. Generally, the INS errors can be approximated by a monotonically-increasing, time-dependent error and a periodic error at the Schuler frequency. These errors can change drastically from one flight to another on the same system since unpredictable errors occur in INS gyros and accelerometers, and the initial alignment, which varies from flight to flight, plays an important role in subsequent INS performance. The alignment sequence, which normallv takes 15 to 20 minutes, includes initializing the INS coordinates, leveling the platform, and gyrocompassing to determine true north. Once the INS is in its navigation mode, any interruption can cause it to lose its navigation capability for the duration of the flight. Much more detailed analyses of inertial systems and their errors are presented by Broxmeyer (1964), Kayton and Fried (1969) and Britting (1971).

- Baro-inertial Loop

In the vertical, no closed loop exists for inertial measurements. However, pressure altitude can be used to limit errors introduced by errors in vertical acceleration. (An offset, or bias in vertical acceleration, when integrated twice, results in an error in altitude that increases with time squared.) At NCAR, the pressure altitude is combined with the vertical acceleration in a third-order loop (see Fig. 3.8) to provide an absolute long-term reference for altitude and vertical velocity. The advantage of a third-order baro-inertial loop (Blanchard, 1971) over a second-order loop system is the elimination of velocity and position error due to bias in the measured acceleration. For the NCAR aircraft (Lenschow, et al., 1978a), a 60-second time constant is used in the mechanization of this loop. This value is based on a compromise between minimizing the effect of high-frequency noise from the pressure altitude measurement (e.g., data system resolution, transducer noise, and pressure line "ringing"); and (1) minimizing the recovery time of the loop for extraneous disturbances (i.e., glitches) and (2) improving the long-term stability of the vertical accelerometer output.

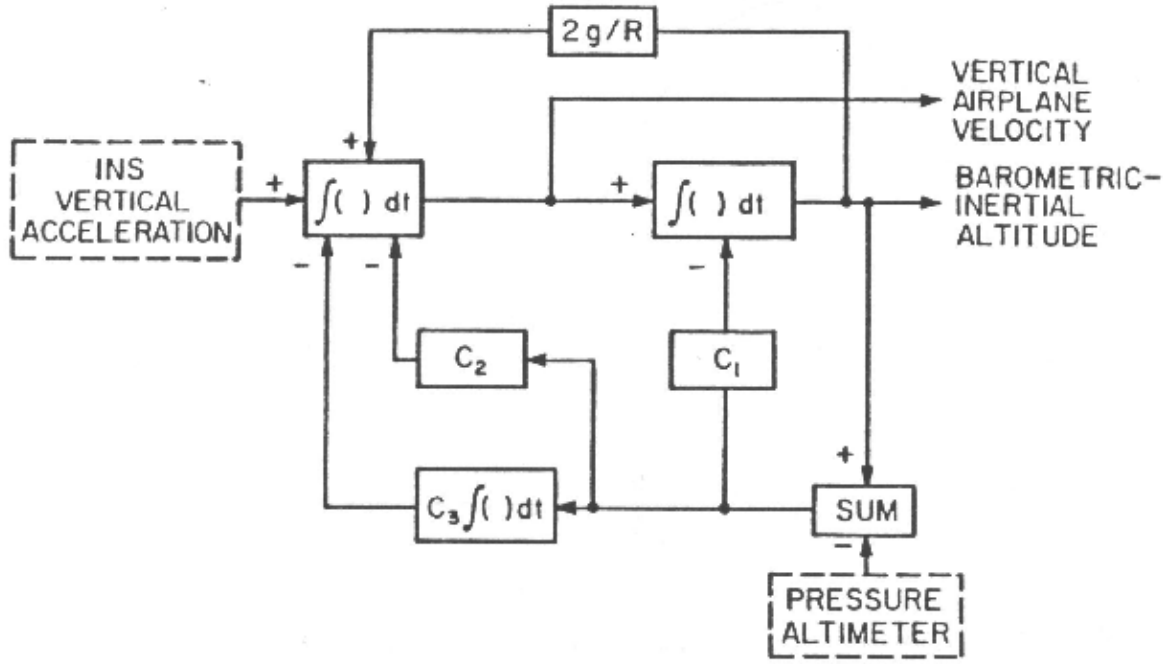

Fig. 3.8. Block diagram of a third-order baro-inertial loop for calculating altitude and vertical airplane velocity from a pressure altimeter and INS vertical airplane acceleration. Feedback loops involving C_1, C_2, and C_3 are set for a time constant of 60 s on NCAR aircraft. The term involving $2g/R$ is a correction for the change of gravity with altitude (R is the distance to the center of the earth).

4. IN-FLIGHT CALIBRATION MANEUVERS

Regardless of where instruments are located and how carefully they are calibrated, errors are likely to be present in the measured variables. Ground tests are not useful for calculating velocity-related errors. Wind tunnel tests are difficult and prohibitively expensive for exact simulation of flight conditions. Therefore, in-flight calibrations play an important role in estimating errors and correcting aircraft measurements.

Because of upwash ahead of the aircraft, the airflow angles (attack and sideslip) and airspeed measured at the tip of a nose boom may differ considerably from the actual values that would be measured far away from the aircraft. The upwash affects not only the sensitivity, but also the zero offset of angle measurements, which, therefore, must also be determined from in-flight calibrations.

Maneuvers used for this purpose involve changes in aircraft speed and attitude angles. The following list summarizes several maneuvers used on NCAR aircraft equipped with an INS and the information that can be obtained from them; examples of these maneuvers are shown in Fig. 4.1:

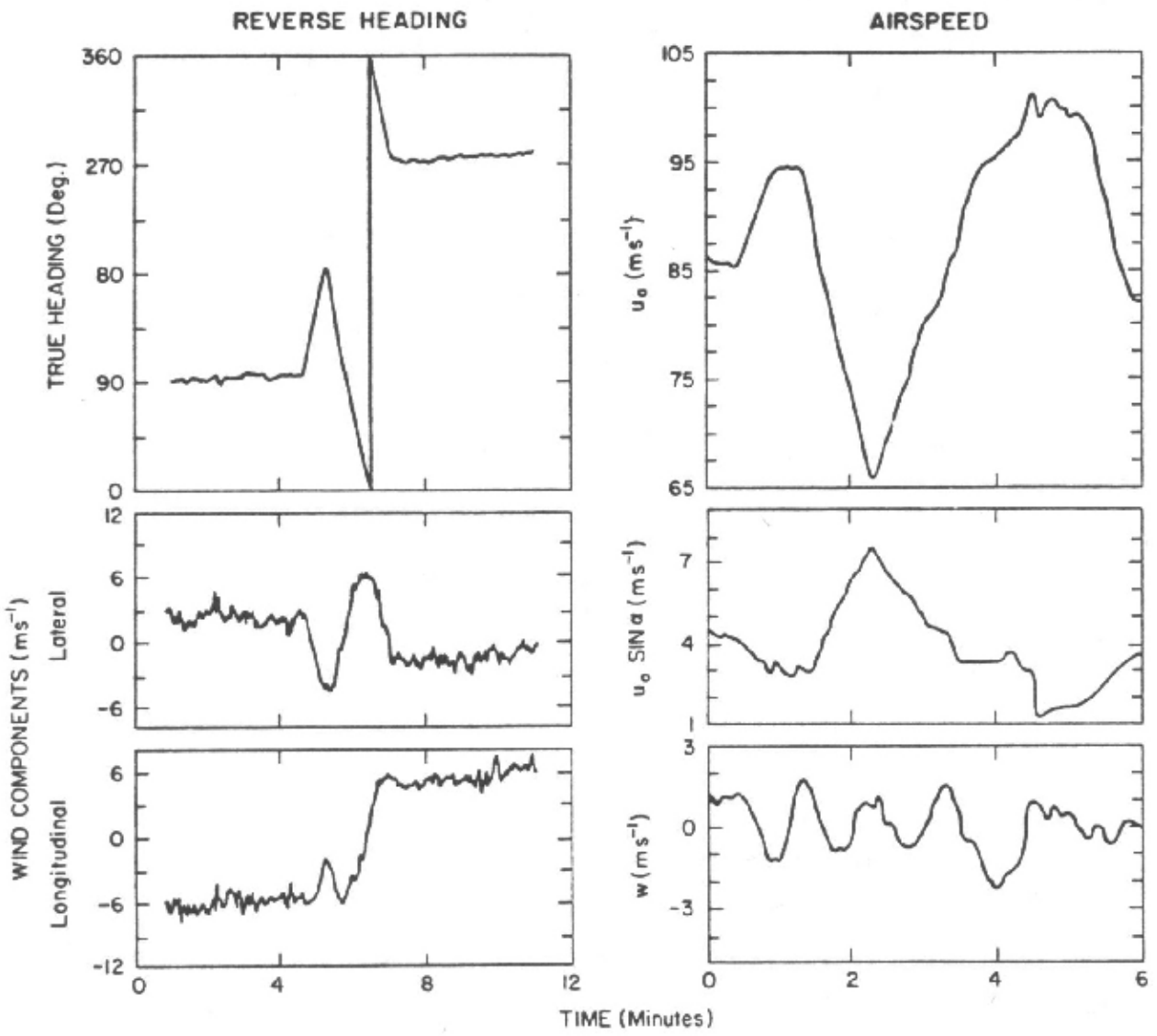

Fig. 4.1a. Examples of reverse heading and airspeed maneuvers used to check the quality of air velocity measurements. The lateral and longitudinal velocity components are measured with respect to the aircraft; therefore, the measured wind should change sign, but not amplitude, after the 180° turn, if the wind field remains constant and is measured without error. An error in airspeed will result in a difference in the amplitude of only the longitudinal component before and after the turn, while an error in the sideslip angle will similarly affect only the lateral component, which simplifies correction procedures. The airspeed maneuver modulates the attack and pitch angles; if pitch angle is measured accurately, the error in attack angle a can be determined by comparing the vertical wind component with respect to the airplane (U_a sin α) with the vertical wind component with respect to the earth (w). In this example, there is little correlation between the two, so the fluctuations in w are presumed to be due to turbulence rather than an inaccurate measurement of α. The airspeed maneuver can also be used to estimate airspeed-dependent errors in other variables and the temperature recovery factor.

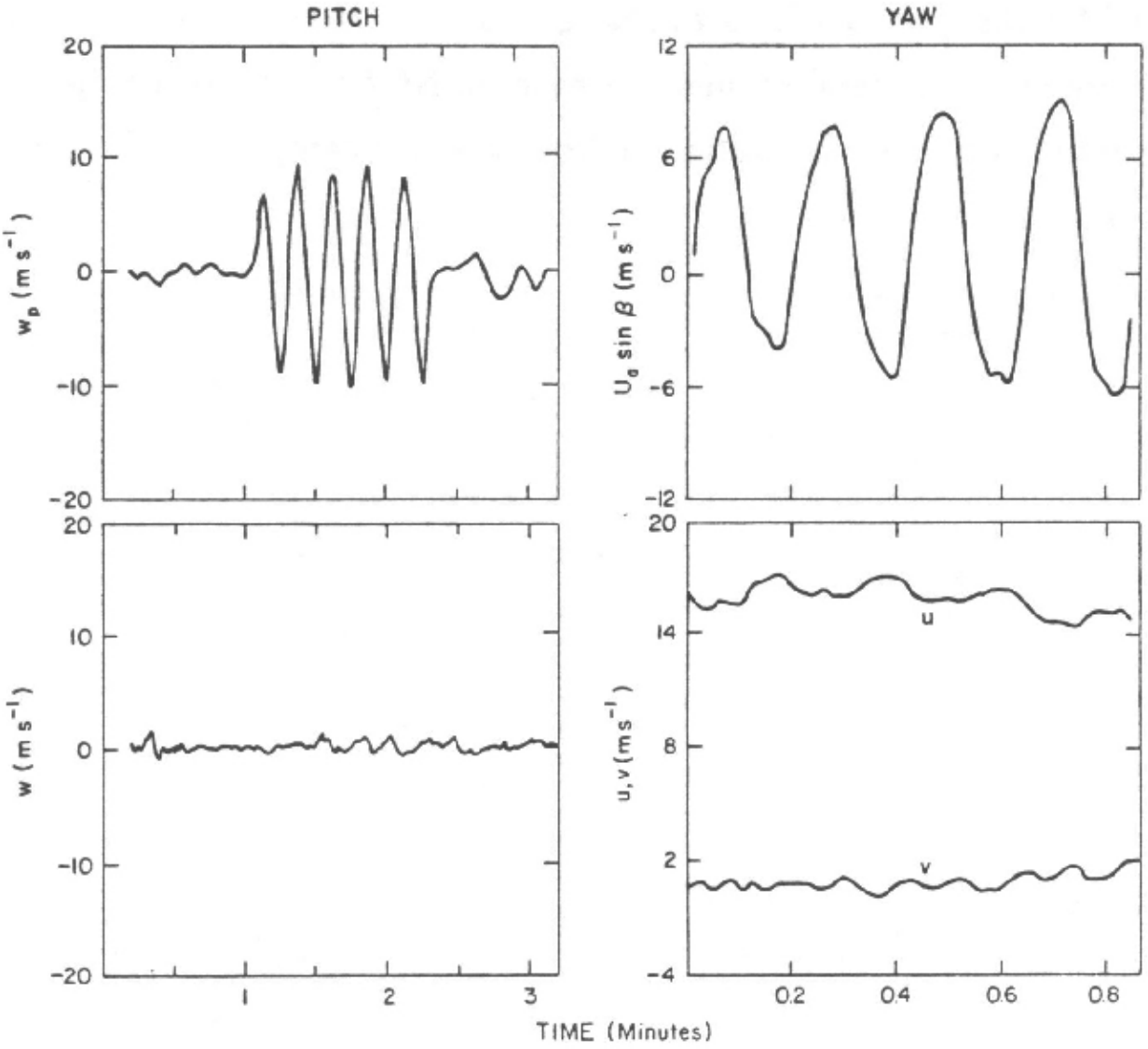

Fig. 4.1b. Examples of pitch and yaw maneuvers. The pitch maneuver is used as an overall check on the accuracy of the *w* measurement; in this example, there is little modulation of *w* during the pitching maneuver, which implies that fluctuations in *w* are measured accurately. Similarly, the yaw maneuver is used as an overall check on the lateral (with respect to the aircraft) component; again there is little modulation of *u* and *v* (in geographic coordinates) by the yawing maneuver.

- **REVERSE HEADING MANEUVER**

  Fly at constant altitude and heading (usually in smooth air above the boundary layer) for several minutes. Then turn 180° by first turning 90° in one direction, then 270° in the other direction at a constant rate so the airplane flies through the same volume of air on its return track. This maneuver modulates the airspeed and sideslip angle errors, since they are measured in the airplane coordinate system. The INS errors are not modulated, however, since they are measured in an inertial frame of reference. If the wind along the flight track is assumed to stay constant during this maneuver, differences in the two wind components between the two headings can be used to independently estimate errors in both airspeed and sideslip angle.

- **SPEED VARIATION MANEUVER**

  Fly at constant altitude and heading, and smoothly vary the aircraft speed from close to stall to close to maximum cruise speed. Since the lifting force on the aircraft is directly proportional to the attack angle and the square of the airspeed, modulating airspeed also modulates attack angle. For level flight, $w_p = 0$ in (2.11); if w, is small, $\alpha = \theta$. Thus, α can be calibrated in flight by this technique, provided that θ is

measured accurately. The attitude angle transducers, in contrast to airflow angle sensors, can be accurately calibrated in the laboratory.

If airspeed is measured incorrectly, temperature may also be affected. Temperature recovery factors (B.8) can also be measured or corrected with this maneuver, since airspeed variations modulate the measured temperature because of dynamic heating effects. Any other measurements affected by either airspeed or attack angle variations are also modulated by this maneuver.

- **PITCH MANEUVER**

  Vary the aircraft elevator angle while holding the heading constant to obtain a sinusoidal pitching motion with a period of 10 to 20 s and a maximum rate of ascent and descent of 2.5 to 4 m/s. This maneuver modulates vertical airplane velocity, w_p; airspeed, U_a; and, to a lesser extent, attack angle, α. If any of these variables have significant errors, a periodic error in vertical air velocity should be evident. Since the terms do not have the same phase angle, in practice it is often possible to determine which of the variables is in error simply by determining the phase of the error in w and comparing it with the phase of w_p, θ, U_a and α. This maneuver also can be used to detect dynamic errors in static pressure or rate-of-climb instruments by comparing their outputs with the integrated lNS vertical acceleration.

- **YAW MANEUVER**

  Vary the aircraft rudder angle while holding the roll and altitude constant to obtain a sinusoidal skidding or sideslip motion with a period of about 10 s and a maximum amplitude of about 2° sideslip. This maneuver modulates heading ψ, horizontal airplane velocity components u_p and v_p, and β. As with the pitch maneuver, errors in any of these variables cause a periodic variation in the horizontal wind velocity.

  On the NCAR aircraft, the system performance is judged to be satisfactory if the vertical air velocity error is less than 10% of the vertical airplane velocity for the pitch maneuver, and the lateral air velocity component is less than 10% of U_a sin β for the yaw maneuver.

  We estimate that short-term (i.e., not including long-term INS drift) velocity errors can be reduced to < 0.3 m/s by in-flight calibrations, which agrees well with the analysis by Nicholls (1983).

- Use of Aircraft Response Characteristics

  An alternative to measuring all the components of V_a and the three attitude angle in order to obtain V is to measure the response of the aircraft to fluctuations in the air velocity and use the aircraft transfer function (i.e., the ratio of the airplane response to the input forcing function) to help estimate the air velocity. This process, however, has inherent limitations. First, the airplane transfer function is not known exactly; furthermore, it depends upon the airplane's mass, which is not constant with time because of fuel consumption. Second, the aircraft cannot respond to high-frequency variations in the air velocity. Third, the airplane responds indistinguishably to both horizontal and vertical gusts. Nevertheless, for some applications (e.g., Lenschow, 1976), useful results can be obtained by this technique. This approach was used by Bunker (1955) for turbulence flux measurements, and more recently by Kyle et al. (1976) to estimate updraft profiles in thunderstorms.

  An intermediate approach, which is considerably more accurate, is to measure the airspeed and pitch angle of the aircraft and use its aerodynamic characteristics to calculate angle of attack, from which the vertical air velocity can be obtained. This approach is discussed by Kelly and Lenschow (1978). Here again, the accuracy depends upon aircraft flight characteristics and response time.

5. LIMITATIONS OF AIR MOTION MEASUREMENTS

As with all physical measuring systems, there are limitations, both in the accuracy of the measurement and in the bandwidth (range of wavelengths) over which air velocity can be measured. Furthermore, the limitations are

somewhat different for different velocity components. The horizontal velocity error, for example, has two components: a cyclic component with a period of 84.4 min and a nonperiodic component that usually increases with time. A typical navigational accuracy of the INS is approximately 0.5 m/s. Because of the periodic component, the velocity error for a position error rate of 0.5 m/s is usually larger than 0.5 m/s/h (or 1 kt/h). Exact numbers cannot be specified, since sources of error are multifarious. Some of these are the following:

- The length of the initial alignment time.
- The alignment environment (movement inside the airplane can degrade the alignment by disturbing the platform).
- The flight pattern and turbulence during the flight (and perhaps even the condition of the runway).
- Incorrect biases on the gyroscopes.
- Random changes in instrument performance.

In the vertical direction, the airplane velocity error is limited by using the measured pressure altitude as a long-term reference. Since this is a relatively accurate and stable reference, the vertical velocity of the airplane can be measured to better than 0.1 m/s if horizontal pressure gradients are not unusually large. The wind component along the longitudinal axis of the airplane is obtained from the difference between the airplane true airspeed and the INS-measured longitudinal airplane velocity. Since the airplane speed is usually several times the wind speed, this involves a small difference of two large numbers (the faster the airplane flies, the larger the numbers). Because of the upstream effects of the air flowing around the airplane and the sensor-mounting structures, the Pitot-static and static pressure measurements used in the true airspeed calculation must be empirically corrected. This is done by:

- tower fly-bys,
- flying in opposite directions through a volume of air (reverse heading maneuver) with the wind speed assumed to be constant and removing any observed difference in wind speed along the flight path by adjusting the pressure calibration, and
- the trailing cone method. (The trailing cone method {Brown, 1985 } employs a 30 m long section of tubing 0.95 cm in diameter trailing behind the aircraft with an aerodynamically shaped cone attached to the end for stabilization. The static pressure is obtained from four rings of pressure ports 2.1 m ahead of the cone. This method can be used at all normal research speeds and altitudes.)

Because of the small angles involved in measuring the airflow angles (a change of 0.1° at an airspeed of 100 m/s is equivalent to a change of 17 cm/s in the lateral or vertical air velocity) and the upstream effects of flow around the airplane, the absolute calibration of the airflow angle measurement is (as discussed in Section 3.1.1) dependent upon flight tests rather than laboratory calibrations. An additional problem is the dependency of the measurement on the shape of the sensor. For example, if a new port or radome is used, or if a port becomes dented or scratched, the bias of the sensor may change significantly.

The vertical wind component measurement has an additional constraint. Flight tests cannot determine a mean absolute vertical air velocity. One approach is to assume that the vertical velocity is zero over a particular segment of a flight and reference the velocity measurement to this. It should be kept in mind, however, that this is not an absolute mean vertical velocity and furthermore that the vertical air velocity averaged over a path of longer than a few kilometers may be too small to be measurable.

Some of the drift in the vertical air velocity measurement may, under certain conditions, be reduced by using the airplane itself as a probe. This amounts to calculating the attack angle from the lift characteristics of the airplane. This can only be done by flying with constant airplane power without turns and keeping track of the airplane's weight. But even this technique does not provide an absolute mean vertical air velocity.

Because of these limitations, a "quick look" at the data processed immediately after a flight may not reveal offsets in both the lateral and vertical air velocity components. The lateral velocity offset is removed by comparing wind measurements along reciprocal headings. The vertical velocity component offset can only be approximately removed by assuming that the vertical velocity component is zero along some portion of the flight track. A further problem that should be kept in mind is the degradation in the accuracy of the air velocity measurement during turns or other abrupt changes in aircraft attitude. Although the equations used to calculate the air velocity are exact in the sense that no significant terms are omitted and small angle approximations are not used, system errors are accentuated in turns for the following reasons:

1. The heading may not be sampled frequently enough during rapid turns to provide sufficient resolution for instantaneous wind messurements.
2. The air-sensing probes are not as accurate and flow distortion effects may become more important at the larger airflow angles encountered during rapid turns.

Thus far we have discussed mainly factors that affect the long-wavelength measurement of air velocity. The primary limitations at short wavelengths are vibration and frequency response limitations of the pressure lines. For the Rosemount probe, which is mounted on a nose boom protruding several meters in front of the airplane, nose-boom vibration is a limitation. The location of the air-sensing probe is a compromise between measuring in a region of minimal perturbation of the airflow by the airplane and maintaining a rigid coupling between the air-sensing probe and the INS.

This discussion is summarized in Table 2. Keep in mind that these numbers represent our present capabilities. In some cases, we expect improvements or some relaxation of limits in the future. An example is the improvement in horizontal wind measurement that is possible by updating the INS with external position or velocity information (e.g., LORAN C or other radio navigation). These potential improvements await further testing and software development.

Table 2
Present Specifications of Air Velocity Component Measurement Accuracies

Airplane	Normal True Airspeed Range (m/sec)	Upper Limit Frequency Response (Hz)	Accuracy of Wind Components	
			(Relative) Short-Term (*u*,*v*,*w*) (< 10 min) (m/s)	(Absolute) Long-Term (horizontal,*u*,*v*) (m/s, t in hours)
Electra	90-125	10	±0.1	±(1.0 + 0.5t)
Sabreliner	140-220	10	±0.1	±(1.0 + 0.5t)
King Air	70-100	10	±0.1	±(1.0 + 0.5t)
t = time in hours from start of flight.				

The level of accuracy summarized in Table 2 is useful for a wide variety of research objectives but is not sufficient for all proposed applications. One class of observations for which this accuracy is not sufficient is measurement of the integrals of velocity components around closed paths. Divergence $(\partial w/\partial z = (1/A)\int \vec{v}\cdot\vec{n}d\ell)$ and vorticity $(\zeta = (1/A)\int \vec{v}\cdot d\vec{\ell})$ are examples of this type of measurement. Ching (1975) has used this integral approach to estimate the drag coefficient ($\mathbf{C_D}$) from the vorticity equation, with the result

$$C_D(z) = \frac{-\int_o^h (d\eta/dt)dz + \eta w(h)}{\vec{k}\cdot curl(\vec{v}\,|v|)_z} \qquad (5.1)$$

where

h is the height of the boundary layer,
$\eta = \zeta + f$
f is the Coriolis parameter.

We note that by Stokes' theorem, $\vec{k} \cdot curl(\vec{v}|v|) = (1/A) \int |v| \vec{v} \cdot d\vec{\ell}$. Thus all terms in (5.1) involve integrals of velocity components (or products of velocities) around a closed path.

The errors in divergence or vorticity are due either to errors in the air velocity measured in the airplane coordinate system or in the velocity and attitude angles measured in an earth-based coordinate system with an INS. Constant velocity and heading errors normal to the flight path cancel out for vorticity measurements, and constant velocity errors parallel to the flight path cancel out for divergence measurements. Similarly, constant INS velocity errors integrated around a closed path cancel out for divergence and vorticity measurements. However, the denominator of (5.1) also depends upon the mean wind speed, which does not cancel out for a closed-path integration of a constant error in INS velocity.

Ching (1975) has estimated the terms in (5.1) from Barbados Oceanographic and Meteorological Experiment (BOMEX) ship and rawinsonde data for a station separation, ℓ, of about 5×10^5 m. Typical values that he found for these terms (excluding the time derivative term) in this maritime tropical environment are:

$$\zeta \simeq -0.8 \times 10^{-5} \mathrm{s}^{-1}$$

$$\frac{\partial w}{\partial z}(1,300 \text{ m}) = -0.4 \times 10^{-5} \text{ s}^{-1}$$

$$\vec{k} \cdot curl(\vec{v}|v|) \equiv -0.8 \times 10^{-4} \text{ m s}^{-2}$$

If the airplane is assume to fly around a closed path in the shape of a regular polygon, with n sides of length ℓ, the enclosed area is $(1/4)n\ell^2 cot(\pi/n)$. The ratio of the circumference, C, to the enclosed area, A, is

$$C/A = \frac{4}{\ell} \tan\left(\frac{\pi}{n}\right) = \frac{4n \tan(\pi/n)}{C} \qquad (5.2)$$

The error in divergence or vorticity due to an error in the velocity component normal or parallel to the flight path, ε_v, integrated around the closed flight path, is

$$\varepsilon \cong \frac{\varepsilon_v C}{A} = \frac{\varepsilon_v 4n \tan(\pi/n)}{C} \qquad (5.3)$$

If the error is assumed to be a constant plus a linear function of time,

$$\varepsilon = \frac{(a_0 + a_1 t)4n \tan(\pi/n)}{C} = a_0 \left(1 + \frac{a_1}{a_0} \frac{C}{U_a}\right) \frac{4n \tan(\pi/n)}{C} \qquad (5.4)$$

where U_a, is the airplane velocity.

If the airplane is flown around the same closed path successively in opposite directions, the contribution of the mean velocity error to the divergence of vorticity should vanish. However, the term in the denominator of (5.1) depends upon the mean wind speed, and thus the mean velocity error contribution does not vanish. Therefore, for divergence and vorticity,

$$\varepsilon_1 \cong \frac{4a_1 n \tan(\pi/n)}{U_a}$$

and for the denominator of (5.1),

$$\varepsilon_2 \cong \left(a_0 + \frac{a_1}{a_0}\frac{C}{U_a}\right)\frac{4a_1 n \tan(\pi/n)}{U_a}$$

For the BOMEX case, using the error given in the first paragraph, $n = 4$ and $U_a = 100$ m/s, we have $\varepsilon_1 \equiv 0.2 \times 10^{-4}$/s and $\varepsilon_2 \equiv 0.3 \times 10^{-4}$ m/s. In terms of the estimated values of divergence and vorticity, this is too large by an order of magnitude. The error in the denominator of (5.1), however, seems within reach of present systems. Although the error estimate is conservative, the distance between BOMEX stations may not be optimal, and techniques can be used operationally to reduce this error (e.g., flying around a closed path many times), the fact remains that the current NCAR systems are not capable of routinely measuring divergence or vorticity by the closed-integral method except in extreme cases such as severe weather phenomena, rapidly developing cumuli, or frontal uplifting. Raymond and Wilkening (1982) have measured divergence with NCAR aircraft around developing mountain cumuli; Nicholls (1983) has estimated divergence over the ocean with a system using an INS updated with radio navigation information; and Gultepe et al. (1989) have estimated divergence in a cirrus cloud deck from closed loops flown during a spiral descent.

APPENDIX A

TIME RESPONSE OF THE ROSEMOUNT MODEL 858AJ DIFFERENTIAL PRESSURE PROBE

In order to determine the effect of long tube lengths on the time response of pressure measurements, flight tests were conducted on a Queen Air flying both the Rosemount probe and, for reference, a fixed-vane probe which has a much faster response time (on the order of 0.01 s) for both Pitot pressure and attack angle. None of the variables was altered. The power spectral densities of the attack angle pressure difference, using tube lengths identical to the Sabreliner's (about 5 m), are plotted in Fig. Al. There is little obvious indication of attenuation at high frequencies or of a large resonance peak. Because of this insensitivity, we will not consider attenuation characteristics, but only phase angle differences. Figure A2 shows that the phase angle of the Rosemount Pitot pressure is $\phi \simeq -6f°$, where f is frequency (Hz). In Fig. A3, the phase angle of the Rosemount attack angle differential pressure is $\phi = -9f°$. These results were obtained at a flight level of 790 mb; the absolute dynamic Pitot pressure was about 820 mb.

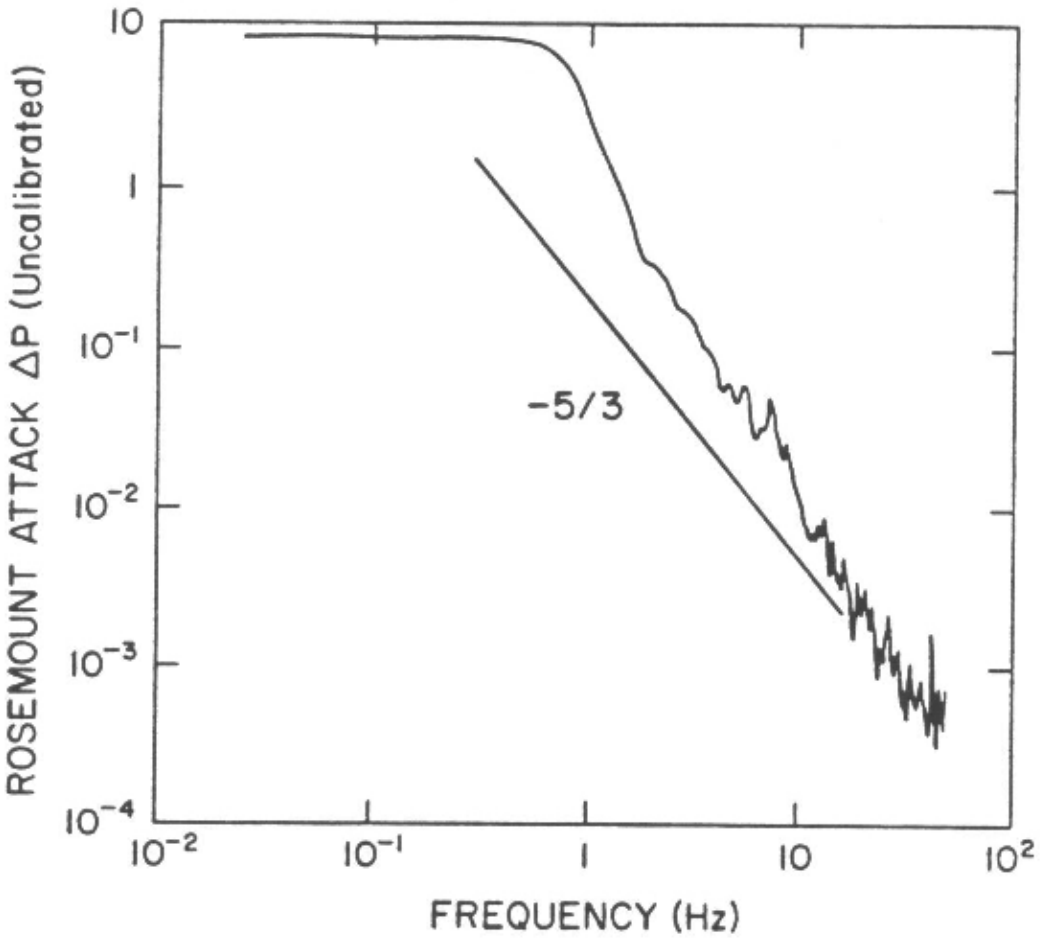

Figure Al. Spectral density of the Rosemount differential pressure probe attack angle output (uncalibrated units). Line of -5/3 slope is drawn for reference. The tube length was about 5 m, and ambient static pressure was about 790 mb.

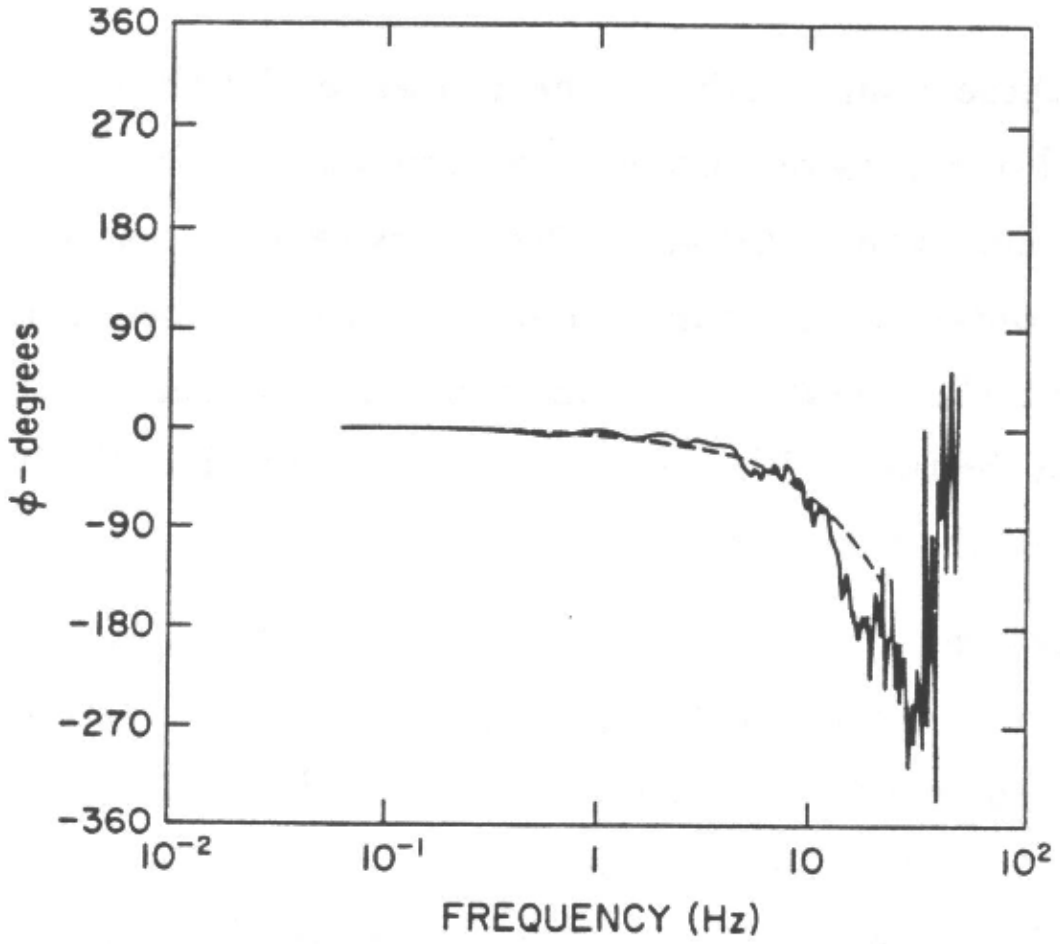

Fig. A2. Phase angle of fixed-vane-probe Pitot pressure versus the Rosemount differential pressure probe Pitot pressure. Negative phase angle means that the Rosemount lags the fixed vane Pitot. Dashed line is a phase lag of $\phi = -6f°$.

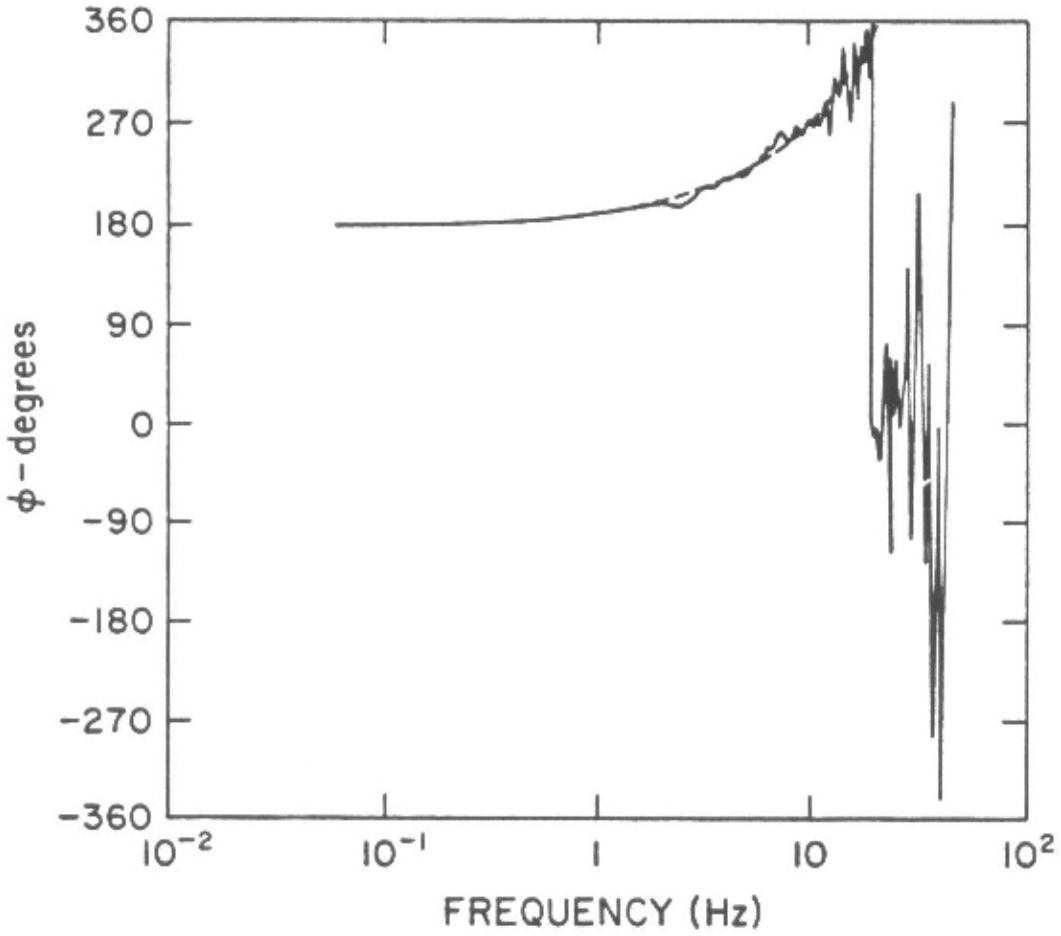

Fig. A3. Phase angle of attack angle differential pressure versus fixed vane. Positive phase angle means that the differential pressure probe lags the fixed vane. Dashed line is a phase lag of $\phi = -9f°$.

We can compare these results with the theoretical results obtained by Iberall (1950) for the attenuation and phase lag of a pressure measurement at one end of a tube with an oscillating pressure applied at the other end. The theory takes into account compressibility and the volume of air contained in the instrument sensing chamber. However, it does not apply exactly to the Sabreliner, system since the tubes are terminated at ports which have a smaller diameter than the tubes. We can make one simplification; the instrument volume is negligible compared to the tube volume.

For the Pitot pressure tube with an assumed diameter of 0.36 cm and a ratio of instrument volume to tube volume of $V_i/V_t = 0$, the theory predicts a phase lag of 22° at 10 Hz. At higher frequencies, the signal is attenuated, and the phase shift continues to increase. The observed phase lag is about 60°. This considerable difference may be because the initial section of the tube is smaller in diameter than the main section. If we assume that this effectively changes V_i/V_t, we find that for a ratio of $V_i/V_t = 0.5$, $\phi = 60°$ at 10 Hz. Alternatively, we can calculate the effective diameter of a tube which has a 60° phase lag at 10 Hz. This turns out to be $d = 0.25$ cm. Recently, the Pitot pressure tube diameter has been changed to 0.14 cm, the same as the flow angle port diameters; the effect of this modification on the frequency response has not yet been tested. We would not expect it to be the same as the flow angle frequency response, since the diameter of the interior tubing is different.

For the attack angle differential pressure, if we use a tube diameter of 0.14 cm, the theoretical phase angle is about 90° at 10 Hz which agrees well with the observed phase lag.

Obviously, the effect of a varying diameter in the pressure lines is significant. Since Iberall (1950) does not cover such complex geometry, we can only use his results for qualitative comparisons with the observed results. However, we can apply the theory quantitatively to estimate what happens when we vary the geometry or the

fluid properties. In particular, the Sabreliner typically flies much higher than the altitude of these test results. The time constant of the pressure lines is inversely proportional to the static pressure. At 12,200 m (40,000 ft), the atmospheric pressure is 188 mb. We add to this 80 mb for the Sabreliner Pitot pressure. The ratio of the flight test pressure to this pressure is 3.06. Thus, at this level the phase lags for Sabreliner measurements of true airspeed and incidence flow angles are -18f° and -27f°, respectively. At a normal Sabreliner data sample rate of 1 sps, the phase lags for true airspeed and flow angles at 0.5 Hz (the Nyquist frequency) are -9° and -14°, respectively. This should be kept in mind when using the Rosemount probe, particularly for calculating cospectra or covariances.

APPENDIX B

CALCULATION OF TRUE AIRSPEED

D. H. Lenschow, P. Spyers-Duran, and C. Friehe[1]

The true airspeed of the aircraft, U_a, is calculated from measurements of the Pitot-static pressure difference, $q = P_t - P_s$,; the static pressure, P_s; and the total air temperature, T_t, using Bernoulli's equation for the conservation of energy of a perfect gas undergoing an adiabatic process,

$$U_1^2/2 + C_pT_1 = U_2^2/2 + C_pT_2 \qquad \text{(B.1)}$$

where C_p is the specific heat at constant pressure. The dynamic pressure, P_t is normally measured at the forward-facing front port of a Pitot tube. The static pressure, P_s may be measured either at the static ports of a Pitot-static tube or at static ports on the aircraft fuselage. Applying this equation to the aircraft, $U_2 = 0$, $T_2 = T_t$ $U_1 = U_a$, and $T_1 = T_s$. Thus,

$$U_a^2 = 2C_p(T_t - T_s) \qquad \text{(B.2)}$$

For an adiabatic process,

$$T_s = T_t(P_s/P_t)^{\frac{\gamma-1}{\gamma}} \qquad \text{(B.3)}$$

where $\gamma \equiv C_p/C_v$ and C_v is the specific heat at constant volume. By substituting this into (B.2),

$$U_a^2 = 2C_pT_t\left[1 - \left(\frac{P_s}{P_t}\right)^{\frac{\gamma-1}{\gamma}}\right] \qquad \text{(B.4)}$$

or equivalently, using T_s,

$$U_a^2 = 2C_pT_s\left[\left(\frac{P_t}{P_s}\right)^{\frac{\gamma-1}{\gamma}} - 1\right] \qquad \text{(B.5 and B.6)}$$
$$= \gamma RT_sM^2$$

where

$$M^2 \equiv \frac{2}{\gamma - 1}\left[\left(\frac{P_t}{P_s}\right)^{\frac{\gamma-1}{\gamma}} - 1\right] \qquad \text{(B.7)}$$

and $R = C_p - C_v$ is the gas constant. The Mach number, M, is equal to the ratio of the true airspeed to the speed of sound.

Table B1
Correction factors (*COR*) for specific heat of air at constant pressure C_p, and ratios of moist air to dry air Mach numbers (M) and true airspeeds (U_a) for several values of dewpoint temperature (T_d). The values of r are saturated mixing ratio at a static pressure of 1,000 mb.

T_d (°C)	r ($\times 10^3$)	e (mb)	*COR*	$\frac{M\ (moist\ air)}{M\ (dry\ air)}$	$\frac{U_a\ (moist\ air)}{U_a\ (dry\ air)}$	% change in U_a
0	3.84	6.11	1.0084	1.00071	1.0017	0.17
10	7.76	12.27	1.0160	1.00144	1.0033	0.33
20	14.95	23.27	1.0300	1.00274	1.0067	0.67
30	27.69	42.43	1.0542	1.00476	1.012	1.2

In practice, neither the total nor the ambient temperature is measured. Instead, the measured temperature, T_r lies between T_t and T_s. Therefore, a recovery factor,

$$r \equiv \frac{T_r - T_s}{T_t - T_s} \qquad \text{(B.8)}$$

is determined for each thermometer on the airplane. This factor is assumed to be constant and independent of humidity. Substituting (B.8) into (B.2),

$$T_s = \frac{T_r}{r\left(\frac{P_t}{P_s}\right)^{\frac{\gamma-1}{\gamma}} + (1 - r)} \qquad \text{(B.9)}$$

and finally, substituting (B.7) and (B.9) into (B.6),

$$U_a^2 = \frac{\gamma R M^2 T_r}{r\left(\frac{\gamma-1}{2}\right)M^2 + 1} \qquad \text{(B.10)}$$

The values of γ and C_p are not completely independent of humidity. The water vapor dependence of C_p (cal/g/K) is given by (List, 1971):

$$\begin{aligned} C_p &= 0.2399 + 0.4409r + \Delta C_p \\ &= 0.2399[1 + 1.838r + 4.168\Delta C_p] \\ &= 0.2399 \cdot COR \end{aligned} \qquad \text{(B.11)}$$

where ***r*** is water vapor mixing ratio (g H_2O/g air) and ΔC_p is a function of T_s, P_s and ***r***. The value of ***COR***--the moisture correction term--is given in Table B1 for moist air with dew points from 0 to 30°C.

The effect of water vapor on γ is given by (List, 1971)

$$\gamma = \gamma_o - 0.1\frac{e}{P_s} = \gamma_o\left[1 - 0.07129\frac{e}{P_s}\right] \qquad \text{(B.12)}$$

where ***e*** is the partial pressure of water vapor and ***r*** = 1.4028 for dry air. Estimates of the moist air corrections to Mach number and true airspeed are also given in Table B1.

---

[1] Dept. of Mechanical Engineering, University of California at Irvine, Irvine, CA 92717

References

Andersen, N.Y., 1955: An Estimate of the Probable Behavior of the Cornell Aeronautical Laboratory Yaw-Pitch Pitot-Static Probe in the Mach Number Range of 0.3 to 2.0. *Report No. IH-933-P-1*. Cornell Aeronautical Laboratory, Inc., 33 pp.

Axford, D.N., 1968: On the accuracy of wind measurements using an inertial platform in an aircraft, and an example of a measurement of the vertical mesostructure of the atmosphere. *J. Appl. Meteorol,* **7**, 645-666.

Blanchard, R.L., 1971: A new algorithm for computing inertial altitude and vertical velocity. *IEEE Trans. Aerosp., Electron. Syst.*, **AES-7**, 1143-1146.

Britting, K.R., 1971: *Inertial Navigation Systems Analysis*. John Wiley & Sons, Inc., New York, NY, 249 pp.

Brown, E.N., C.A. Friehe, and D.H. Lenschow, 1983: The use of pressure fluctuations on the nose of an aircraft for measuring air motion. *J. Clim. Appl. Meteor.*, **22**, 171-180.

Brown, E.N., 1985: Calibration of the NCAR Sabreliner Research Static Pressure Source with a Trailing Cone Assembly. *Technical Note NCAR/TN-253+EDD*. NCAR, Boulder, Colo., 16 pp.

Broxmeyer, C., 1964: *Inertial Navigation Systems*. McGraw-Hill Book Co., New York, N.Y., 254 pp.

Bunker, A.F., 1955: Turbulence and shearing stresses measured over the North Atlantic by an airplane acceleration technique. *J. Meteorol.*, **12**, 445-455.

Ching, J.K.S., 1975: Determining the drag coefficient from vorticity, momentum, and mass budget analysis. *J. Atmos. Sci.*, **32**, 1898-1908.

Etkin, B., 1959: *Dynamics of Flight*. John Wiley & Sons, Inc., New York, N.Y., 519 pp.

Gultepe, I., A.J. Heymsfield and D.H. Lenschow, 1989: A comparison of vertical velocity in cirrus obtained from aircraft and lidar divergence measurements during FIRE. *J. Atmos. and Oceanic Tech.*, in press.

Iberall, A.S., 1950: Attenuation of oscillatory pressures in instrument lines. *J. Res. Nat. Bur. Stand.*, **4J**, 85-108.

Johnson, H.P., D.H. Lenschow, and K. Danninger, 1978: A new fixed vane for air motion sensing. In *Preprints, Fourth Symposium on Meteorological Observations and Instrumentation*. 10-14 April, Denver, Colo., American Meteorological Society, Boston, Mass., 467-470.

Kayton, M., and W.R. Fried, 1969: *Avionics Navigation Systems*. John Wiley & Sons, Inc., New York, N.Y., 666 pp.

Kelly, T.J., and D.H. Lenschow, 1978: Thunderstorm updraft measurements from aircraft. In *Preprints, Fourth Symposium on Meteorological Observations and Instrumentation*, 10-14 April, Denver, Colo., American Meteorological Society, Boston, Mass., 474-478.

Kyle, T.G., W.R. Sand, and D.J. Musil, 1976: Fitting measurements of thunderstorm updraft profiles to model profiles. *Mon. Weather Rev.*, **104**, 611-617.

Lenschow, D.H., 1971: Vanes for sensing incidence angles of the air from aircraft. *J. Appl. Meteorol.*, **10**, 1339-1343.

Lenschow, D.H., 1972: The Measurement of Air Velocity and Temperature Using the NCAR Buffalo Aircraft Measuring System. *Technical Note TN/STR-74*, NCAR, Boulder, Colo., 39 pp.

Lenschow, D.H., 1976: Estimating updraft velocity from an airplane response. *Mon. Weather Rev.*, **104**, 618-627.

Lenschow, D.H., C.A. Cullian, R.B. Friesen, and E.N. Brown, 1978a: Status of air motion measurements on NCAR aircraft. In *Preprints, Fourth Symposium on Meteorological Observations and Instrumentation*, 10-14 April, Denver, Colo., American Meteorological Society, Boston, Mass., 433-438.

List, R.L., 1971: *Smithsonian Meteorological Tables*. Smithsonian Institution, Washington, D.C., 527 pp.

Nicholls, S., 1983: *An Observational Study of the Mid-latitude, Marine Atmospheric Boundary Layer*. Ph.D. dissertation, University of Southampton, U.K., 307 pp.

Raymond, D.J., and M.H. Wilkening, 1982: Flow and mixing in New Mexico mountain cumuli. *J. Atmos. Sci.*, **38**, 2211-2228.

Wyngaard, J.C., L. Rockwell and C.A. Friehe, 1985: Errors in the measurement of turbulence upstream of an axisymmetric body. *J. Atmos. Ocean. Tech.*, **2**, 605-614.

For Further Reading:
Lenschow, D.H., Ed., 1986: *Probing the Atmospheric Boundary Layer: Aircraft Measurements in the Boundary Layer*. American Meteorological Society, Boston, Mass., 39-55.

RAF Technical Bulletins / ***RAF Home Page*** / ***EOL Home Page*** / ***NCAR Home Page***

Last update: Mon Nov 12 18:35:01 MST 2001